Journal of Experimental Nanoscience
Publication details, including instructions for authors and subscription information:
http://www.informaworld.com/smpp/title~content=t716100757

A simple atomic force microscopy method for the visualization of polar and non-polar parts in thin organic films

A. Amy Yu[a]; Peter R. Stone[a]; Julie E. Norville[b]; Michael Vaughn[c]; Eden J. Pacsial[d]; Barry D. Bruce[ce]; Marc Baldo[b]; FranÇisco M. Raymo[d]; Francesco Stellacci[a]
[a] Department of Materials Science and Engineering, MIT, Cambridge, MA, USA [b] Department of Electrical Engineering and Computer Science, MIT, Cambridge, MA, USA [c] Department of Biochemistry, Cellular, and Molecular Biology, University of Tennessee at Knoxville, Knoxville, TN, USA [d] Center for Supramolecular Science, Dept. of Chemistry, University of Miami, Coral Gables, FL 33146, USA [e] Center of Excellence in Environmental Biotechnology, University of Tennessee at Knoxville, Knoxville, TN, USA

Online publication date: 28 September 2010

To cite this Article Amy Yu, A. , Stone, Peter R. , Norville, Julie E. , Vaughn, Michael , Pacsial, Eden J. , Bruce, Barry D. , Baldo, Marc , Raymo, FranÇisco M. and Stellacci, Francesco(2006) 'A simple atomic force microscopy method for the visualization of polar and non-polar parts in thin organic films', Journal of Experimental Nanoscience, 1: 1, 63 — 73
To link to this Article: DOI: 10.1080/17458080500372290
URL: http://dx.doi.org/10.1080/17458080500372290

Journal of Experimental Nanoscience,
Vol. 1, No. 1, March 2006, 63–73

Taylor & Francis
Taylor & Francis Group

A simple atomic force microscopy method for the visualization of polar and non-polar parts in thin organic films

A. AMY YU†, PETER R. STONE†, JULIE E. NORVILLE‡,
MICHAEL VAUGHN§, EDEN J. PACSIAL¶,
BARRY D. BRUCE§⊥, MARC BALDO‡, FRANÇISCO M. RAYMO¶
and FRANCESCO STELLACCI*†

†Department of Materials Science and Engineering, MIT,
Cambridge, MA, 02139, USA
‡Department of Electrical Engineering and Computer Science, MIT,
Cambridge, MA, 02139, USA
§Department of Biochemistry, Cellular, and Molecular Biology,
University of Tennessee at Knoxville, Knoxville, TN, 37996, USA
¶Center for Supramolecular Science, Dept. of Chemistry,
University of Miami, Coral Gables, FL 33146, USA
⊥Center of Excellence in Environmental Biotechnology,
University of Tennessee at Knoxville, Knoxville, TN, 37996, USA

(*Received August 2005; in final form September 2005*)

Here we present a scanning probe microscopy method that allows for the identification of regions of different polarity (i.e. hydrophilicity) in thin organic films. This technique is based on the analysis of the difference between phase images generated at different applied bias voltages in tapping-mode atomic force microscopy. We show that, without any chemical modification of the microscope tip, it is possible to investigate surface properties of complex macromolecular layers, yielding new insight into the functional properties of the photosynthetic electron transport macromolecular complex, Photosystem I.

Keywords: Atomic force microscopy; Polarity; Organic films

1. Description of the technique

Due to the advances in surface science, a large number of thin organic films, such as molecular self-assembled monolayers (SAMs) or protein layers, have been fabricated [1]. Applications range from molecular electronics to advanced and ultrasensitive bio-sensing [2]. In recent years, it has become clearer that the morphology of these films plays an important role in determining their performances [3, 4]. For example,

*Corresponding author. Email: frstella@mit.edu

Journal of Experimental Nanoscience
ISSN 1745-8080 print/ISSN 1745-8099 online
http://www.tandf.co.uk/journals
DOI: 10.1080/17458080500372290

in order to produce efficient protein biosensors, the conformation of the receptor needs to be known and controlled.

There are a few methods that allow for the identification and analysis of the morphology and conformation of complex organic films. Some only analyse large areas [1] (low spatial resolution); others, based on scanning probe microscopy, have the needed spatial resolution but can only probe topological differences [1]. This is an enormous limitation because, mostly for biological samples, the topological image is complex and typically not interpretable [5]. Even in simple molecular SAMs, the physical phenomena that lead to the topological contrast are sometimes not clear [6]. As a consequence, many groups are trying to extract non-topological information from atomic force microscopy (AFM) images. One of the main efforts relies on the chemical functionalization of AFM tips [7], a successful approach limited by the unknown conformation of the molecules on the tip, and by the constrained molecule/sample combinations. This family of approaches relies on the generation of a map of the interaction forces between molecules on the tip and molecules on the surface; the better the molecular combination (receptor–receptand), the better the results.

A series of scanning probe microscopy techniques have been developed in recent years to produce images that depend on the surface energy of the sample [8]. These approaches tend to have promising applications for the characterization of molecular and biomolecular surfaces. Some techniques map frictional forces derived from the tip–sample interactions [9, 10]. In some cases tip functionalization can improve resolution [7–9]. Biological samples sometimes are too soft for this contact microscopy. Consequently some research focus has shifted towards a series of non-contact microscopy based on surface potential detection [11], namely Kelvin probe microscopy (KPM) [8, 12–14] and electrical force microscopy (EFM) [15]. KPM measures the difference in surface potential between a sample and the tip. It is fundamentally limited in resolution and probes only the outermost surface. EFM is a 'lift mode' technique, in which the tip is raised from the sample and left free to oscillate at its resonant frequency. Phase shifts are generated by electrostatic force fields. In one variation (dynamic contact mode), EFM has been used in contact mode not in tapping mode, thus with the tip in contact with the sample. This configuration enables the charges to better decouple from topological effects [16].

Here, we present a method that, without any molecular tip functionalization, can distinguish between regions with different polarities in an organic sample placed on a conductive substrate. It is an evolution of EFM because it is based on the analysis of the **E**lectrostatically generated **P**hase difference in **T**apping-mode **A**FM (EPTA). In EPTA, the tip is always engaged and never lifted from the sample. This was found to be helpful in generating large phase shift and ultimately in improving lateral resolution. Indeed, here we show images of a protein with 7 nm resolution.

Phase, in AFM, is the delay between the driving piezoelectric crystal oscillations and the tip oscillations. It is known that phase images are maps of the dissipative forces that take place at the tip–sample interface [17–19]. In the case of organic samples, these forces mostly originate in the sample itself. In fact, the tip, typically a single Si crystal, has an almost vanishing imaginary (dissipative) component of its mechanical response. On the contrary, for complex supramolecular (or macromolecular) thin layers,

the sample will have a large conformational freedom (at least compared to the tip) and thus a significant dissipative part in its mechanical response. Upon application of a bias between the tip and the conductive substrate, viscoelastic type of oscillations induced by the strong oscillating local field (note that the field is oscillating because a constant bias is applied between the fixed sample and the oscillating tip) will generate new dissipative channels only in the interacting polar (or charged) parts. This will result in an increase (in absolute value) of the phase response. EPTA is based on the difference between phase images taken at varying electrical biases. Apolar regions in the sample weakly interact with the field and consequently show little phase changes. Polar or charged regions interact strongly with the field, thus changing their phase response. Additional contribution to the EPTA response come from the sample interfacial potential [8] and the condensed water layer that is always present on samples [20, 21]. Both effects amplify EPTA response (the former being much smaller than the latter), being stronger on polar regions [21] of a sample and thus help improve EPTA resolution. Since EPTA is the difference between two phase images, the effect of all other factors that produce phase contrast [19] is eliminated. It should be noted that in EPTA a bias is applied while imaging with the tip engaged on the sample, not after the tip has scanned and has been 'lifted' at a fixed distance from the sample (interleave mode) [22]. Also, all of the parameters (e.g. drive frequency or drive amplitude) used to engage and image at zero bias are left unchanged when imaging at a given voltage.

To test our idea, we prepared two SAMs, one made of molecules terminated with a polar group (6-mercapto-1-hexanol, **MH**, HS-$(CH_2)_6$-OH), and the other made of apolar molecules (1-hexanethiol, **HT**, HS-$(CH_2)_5$-CH_3). Both SAMs were prepared on Au (111) surfaces thermally evaporated on freshly cleaved mica substrates. As shown in figure 1 the application of an electric field mostly does not vary the AFM height images in either case. In general, on both polar and apolar samples, the topological images degrade slightly due to the formation of attractive or repulsive tip–substrate forces that change the cantilever oscillating conditions. This effect is stronger for polar samples. On the contrary, phase images show a different behaviour for the two SAMs. A large phase variation was observed upon application of a bias (+3 V) for the polar SAM (**MH**), while, in the case of the apolar SAM (**HT**), phase variations were hardly observed even upon application of a larger field (+5 V). This confirms that phase values change only in monolayers that can interact with the field. Additionally, for **MH** monolayers, the phase shift (i.e. phase at 0 V *minus* phase at the applied bias) showed a quadratic dependence on the applied bias, as expected for a field–dipole type of interaction [23] (see Appendix A). When EPTA was used to analyse a SAM composed of charged molecules 1-(10-mercaptodecyl)-1′-methyl-4,4′-bipyridinium bis-chloride (see Appendix A for a schematic drawing and synthetic procedure), large phase changes were observed. In this case, the dependence of the phase shifts on the applied bias was asymmetric. Many explanations are possible for this effect, ranging from different mobilities of the charged molecules and their counter-ions, to induced mechanical asymmetry or to the presence of a net charge; further investigations are needed. In any case, we believe that the analysis of the phase shift versus applied bias plot provides additional information in EPTA. Indeed, simpler polar regions will respond almost identically to opposite biases while charged regions will respond preferentially to an opposite tip bias. All of the monolayer

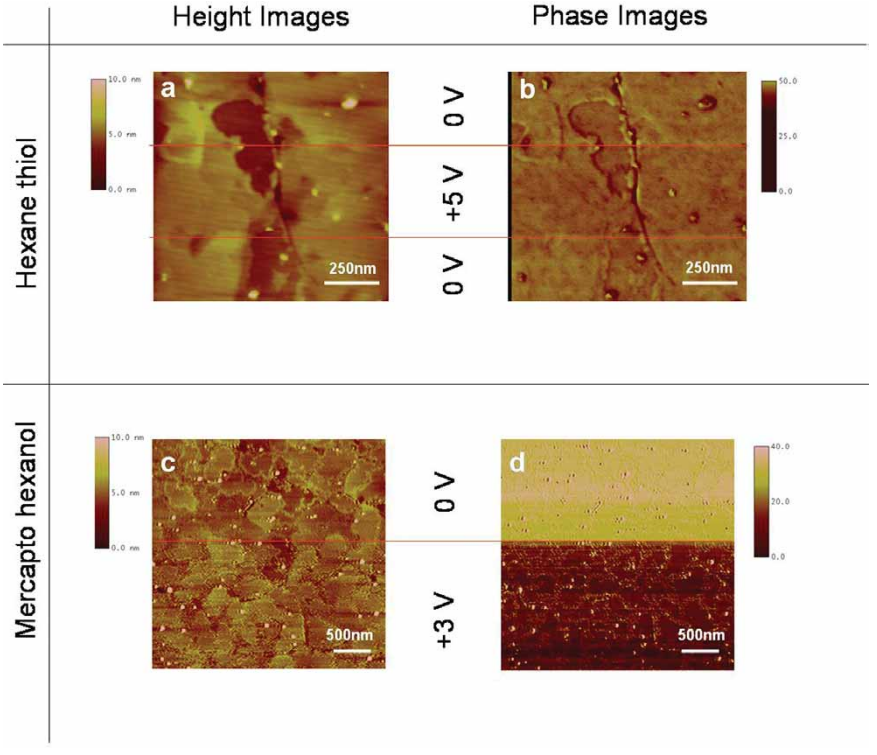

Figure 1. Tapping-mode AFM images of homogeneous monolayers on gold (111) on mica. Height and phase images were collected at the same time on different channels of the microscope. During imaging, while scanning from the top to the bottom, the voltage applied from the tip to the sample was changed as indicated. (**a**) and (**b**) are images of a 1-hexane-thiol (apolar) monolayer. (**c**) and (**d**) are images of a 6-mercapto-1-hexanol (polar) monolayer. Both height images (**a**) and (**c**) do not change upon application of a bias voltage. The phase image of the apolar monolayer (**b**) shows almost no change upon application of a strong bias (5 V). It is evident how the phase images of the polar monolayer (**d**) show a large change upon application of a mild bias (3 V). This figure is available in colour online.

images shown in this paper were obtained in the non-contact regime of tapping-mode AFM (as defined in [17]), but similar results were obtained in the intermittent contact regime (indeed the protein images are made in this latter mode) [17–19].

To further confirm our interpretation of EPTA images, we simulated the setup using a harmonic force balance model originally derived for dynamic modes of AFM [24]. It utilizes a set of equations based on the steady-state sinusoidal motion of the AFM cantilever and it can be solved for AFM imaging variables, such as amplitude, DC offset, and, most importantly, phase. The equations were modified to include the electrostatic forces present in EPTA by introducing a term for the capacitive force. The tip–substrate capacitor was modelled by a sphere–plane geometry [25–26]. First, simulations were run to determine the effect of changing the dielectric constant of a neutral monolayer. Simulation parameters were determined by the specific experimental setup, as well as [24]. The simulation presented in figure 2(a) shows, qualitatively, the quadratic shape of the voltage versus phase shift plots, in good agreement with

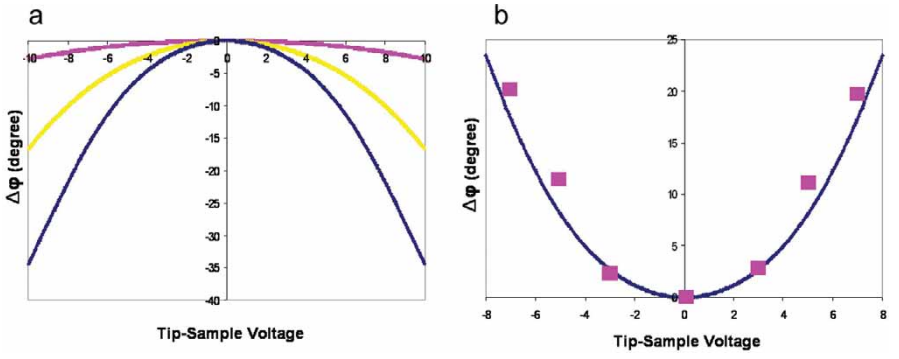

Figure 2. Harmonic force balance simulations for EPTA. **(a)** demonstration of the fundamental operating principle of EPTA by showing the effect of monolayer dielectric constant on phase shift. An increase in the dielectric constant, which corresponds to an increase in the polarity of the monolayer, leads to greater electrostatic dissipation and, hence, a larger phase shift. **(b)** Comparison of simulation and experimental EPTA on a mercapto hexanol monolayer. The simulation is in good agreement with the experimental data. For both **(a)** and **(b)** cantilever parameters were: $k = 35\,\mathrm{N/m}$, $\omega_0 = 300\,\mathrm{kHz}$, $R = 10\,\mathrm{nm}$. This figure is available in colour online.

the experimental results. Importantly, it shows the strong dependence of the parabola's curvature on the sample's dielectric constant. A more quantitative analysis was performed for **MH** monolayers, using a sample dielectric constant of 14, that of tethered hexane molecules (the –SH functionalization was ignored since it is used to anchor the monolayer to the substrate). The results of these calculations are shown in figure 2(b) along with experimental data points. The two data sets are in very good agreement especially at small voltages. Thus, a simple sphere–plane capacitor model can accurately reproduce the behaviour of EPTA.

The main strength of this method is to distinguish polar from apolar regions in a sample. To prove this, we produced a mixed monolayer composed of 1-octanethiol (**OT**, HS-$(CH_2)_7$-CH_3) and 3-mercapto-1-propionic acid (**MPA**, HS-$(CH_2)_2$-COOH) on a Au (111) surface. These two molecules are known to phase-separate into distinct regions when forming SAMs on flat surfaces [27, 28]. While the simple use of phase-imaging allows for the recognition of two different chemical regions, it does not allow for the assignment of the chemical nature of such regions. It is challenging to understand whether there are islands of **MPA** in an **OT** matrix or vice versa. By comparing phase images taken at 0 V and at +2 V (see figure 3a, b and c) we noticed that the phase value of the islands decreased from an average of 11° to an average of 5°, while the matrix (that surrounds the islands) did not change its average value (−11°). This allowed us to understand that the observed phase-separated islands were composed of **MPA** while the matrix was made of **OT** molecules. To the best of our knowledge, this is one of the simplest ways of performing chemical recognition on a sample analysed by AFM with a tip that has no molecular coating.

We used EPTA to investigate the surface properties of a large macromolecular membrane protein complex, Photosystem I (PSI), isolated from chloroplast membranes [30]. A monolayer of this protein complex was unidirectionally oriented on a gold substrate as described in the literature [31]. We imaged the PSI complex at different voltages and found an asymmetric behaviour (figure 3d, e and f). Phase images at +1 V and 0 V

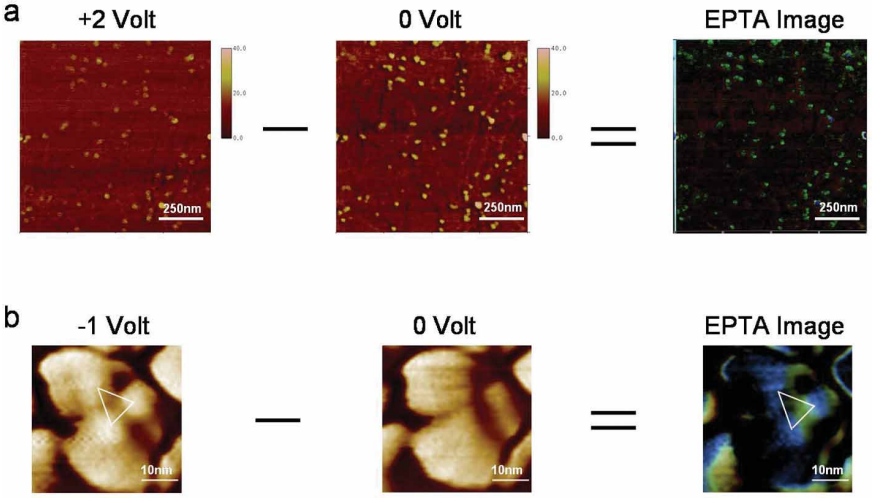

Figure 3. Tapping-mode AFM phase images obtained at different biases and their difference (EPTA image) shown for a mixed monolayer and for a protein system both on Au (111) on mica. (**a**) and (**b**) are phase images of a mixed monolayer composed of 1-octane-thiol and 3-mercapto-propionic acid. Both images show high-phase islands embedded in a low-phase matrix. The difference between these two images (**c**, EPTA image) shows that the islands change their phase value much more than the matrix, indicating that the islands are the most polar part of the sample and thus they are mainly composed of 3-mercapto-propionic acid. (**d**) and (**e**) are phase images of Photosystem I. The difference between these two images (**f**, EPTA image) shows that there are three islands arranged in a triangular fashion and spaced 10 nm. By comparing this experimental evidence with the X-ray determined structure of the protein [29] we could conclude that a trimeric complex was formed. These series of images testify to the versatility and power of EPTA. This figure is available in colour online.

showed almost no difference, while phase images taken at −1 V consistently presented the appearance of three triangularly arranged lobes spaced 10 nm. We assigned the appearance of these lobes to the presence of an electron conductive channel that are potentially the same regions of the complex involved in light-induced charge separation [32]. Moreover, the asymmetry of the PSI image was consistent with the rectifying behaviour of this electron transport protein complex as described in the literature [31]. This new insight into the functional properties of an immobilized monolayer of a macromolecular complex demonstrates the versatility and power of EPTA.

As stated above, the EPTA signal has one contribution that depends on the presence of a water layer on the substrate [20]. In order to estimate the water–viscoelastic response relative to the sample–viscoelastic contribution to the EPTA signal, we made a series of EPTA measurements on an **OT : MPA** mixed SAM at varying relative humidity. We plotted the difference in the average phase value of **MPA** domains at 0 V and +2 V, i.e. the EPTA signal, at various relative humidity values. The values were measured in random order to avoid monotonic build up of the water layer. A linear increase of the EPTA signal with relative humidity was observed, but the intercept of this linear trend at zero relative humidity was not zero but ~2° (figure 4). This is the sample contribution to the EPTA signal. It should be noted that this contribution can be as high as 60% and as low as 30% of the total signal at common relative

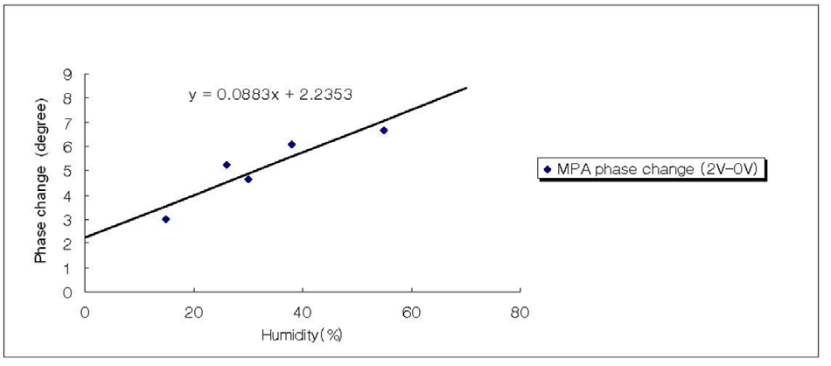

Figure 4. Phase difference versus relative humidity plot in EPTA showing an intercept at 2.2° for zero relative humidity. On the abscissa we plot the difference between the average value of the phase signal of an MPA region in an MPA : OT SAM at 2 V subtracted from its average value at 0 V. The intercept value indicates the sample contribution to the EPTA signal; the extra value is due to the water layer. It should be noted that the OT phase signal does not scale with relative humidity.

humidity conditions. Additionally, the measurements done on Photosynthesis I show that EPTA is able to extract data from samples uniformly coated with a water layer. In order to check whether tip contamination or tip chemical interface had a role in EPTA, we coated our tips with **OT** SAMs and repeated our measurements on **OT : MHA** samples. The results were statistically identical to the ones obtained with uncoated tips.

In order to obtain the results presented above we used a standard commercial AFM and no special modification of hardware, software, or complex tip was required. We thus believe that this new and novel analysis method could be widely adopted with little additional investments by many laboratories worldwide. In conclusion, here we have shown a new technique (EPTA) able to extract chemical information about a sample without the need of tip functionalization.

2. Experimental section

All AFM images were obtained using a Digital Instrument MultiMode Nanoscope IIIa, using both an E and a J scanner. Phase values were obtained though a Quadrex module, known to generate absolute phase values. All experiments presented in the paper were performed using Veeco NanoprobeTM tips (Model #: RTESP; length 125 μm; resonance frequency ~300 kHz) coated with a 5 nm thick thermally evaporated chromium gold layer, except mixed monolayer imaging, that was done using Veeco NanoprobeTM conductive tips (Model #: OSCM-PT; length 240 μm; resonance frequency ~70 kHz). The choice of the tip was not optimized, and depended on availability of tips in the laboratory. Relative humidity was controlled by placing the whole instrument in a closed chamber provided with a humidity control setup.

All samples were prepared on gold (111) thermally evaporated on freshly cleaved mica purchased from Molecular Imaging and used as received. The samples were

mounted on a magnetic sample holder and double-sided conductive tape was used to ensure a conductive path from the gold to the holder. Average resistance was 500 kΩ.

Voltage was applied from the tip to the sample through the microscope; specifically we used the feature "tip bias/analog 2" in the Nanoscope software.

6-mercapto-1-hexanol (**MH**), 1-hexanethiol (**HT**), 3-mercapto-propionic acid (**MPA**), 1-octanethiol (**OT**) and all of the organic solvents used in experiments were purchased from Aldrich and used as received. Millipore water with high purity ($\rho =$ 18.6 MΩ cm) was used to prepare and purify the samples. **MH** was prepared from a 1 mM water solution. **HT** and **MPA**/**OT** (95 : 5 molar ratio) monolayers were prepared from a 1 mM ethanol solution. All monolayers were obtained by overnight immersion and thorough rinsing with multiple solvents. Protein samples were prepared as described in [31].

Appendix A

A.1. *Synthetic procedures*

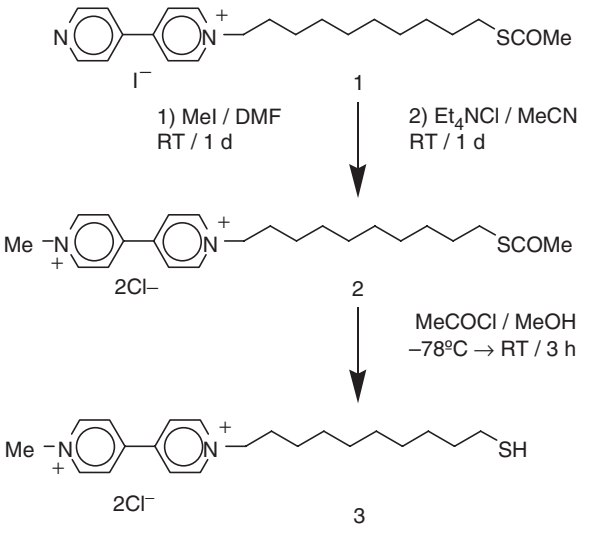

A.1.1. General methods. Chemicals were purchased from commercial sources and were used as received. DMF was dried on 4 Å molecular sieves. MeCN was distilled over CaH_2. MeOH was distilled over Na. Thin layer chromatography (TLC) was carried out on aluminium sheets coated with silica gel 60 F_{254}. Melting points (mp) were determined with an Electrothermal 9100 and are uncorrected. Fast atom bombardment mass spectra (FABMS) were recorded with a VG Mass Lab Trio-2 using 3-nitrobenzyl alcohol as matrix. Nuclear magnetic resonance (NMR) spectra were recorded with a Bruker DPX 300.

1-(10-acetylsulfanyldecyl)-1′-methyl-4,4′-bipyridinium bis-chloride 2. A solution of **1** (100 mg, 0.2 mmol) and MeI (2.28 g, 16 mmol) in DMF (1.5 mL) was stirred for 1 d

at ambient temperature. The solvent was distilled off under reduced pressure and the residue was crystallized from MeCN (7 mL). The resulting solid was suspended in MeCN (3 mL), combined with a saturated MeCN solution of Et_4NCl (5 mL), stirred at ambient temperature for 1 d and filtered to give **2** (105 mg, 82%) as a white solid; mp = 226–230°C (dec.); FABMS: $m/z = 386$ $[M-2Cl]^+$; ^{1}H-NMR (CD_3OD): $\delta = 9.29$ (2H, d, $J = 7$ Hz), 9.19 (2H, d, $J = 7$ Hz), 8.58–8.78 (4H, m), 4.75 (2H, t, $J = 8$ Hz), 4.53 (3H, s), 2.84 (2H, t, $J = 7$ Hz), 2.29 (3H, s), 1.99–2.18 (2H, m), 1.21–1.62 (14H, m); ^{13}C-NMR (CD_3OD): $\delta = 197.68$, 151.23, 151.01, 148.02, 147.10, 128.37, 128.01, 63.33, 32.53, 30.74, 30.53, 30.37, 30.08, 29.81, 29.73, 27.18.

1-(10-mercaptodecyl)-1′-methyl-4,4′-bipyridinium bis-chloride 3. Acetyl chloride (42 µl, 0.6 mmol) was added dropwise to a solution of **2** (38 mg, 0.08 mmol) in degassed MeOH (10 mL) maintained at –78°C under N_2. After 10 min, the mixture was allowed to warm up to ambient temperature in 3 h. The solvent was distilled off under reduced pressure to afford **3** (33 mg, 99%) as a red solid; mp = 223–224°C (dec.); FABMS: $m/z = 344$ $[M-2Cl]^+$; ^{1}H-NMR (CD_3OD): $\delta = 9.28$ (2H, d, $J = 7$ Hz), 9.19 (2H, d, $J = 7$ Hz), 8.65–8.69 (4H, m), 4.75 (2H, t, $J = 8$ Hz), 4.53 (3H, s), 2.48 (2H, t, $J = 7$ Hz), 2.00–2.20 (2H, m), 1.53–1.66 (2H, m), 1.28–1.42 (12H, m); ^{13}C-NMR (CD_3OD): $\delta = 151.48$, 151.20, 148.16, 147.24, 128.43, 128.07, 63.49, 35.27, 32.67, 30.59, 30.52, 30.24, 30.22, 29.46, 27.34, 25.07.

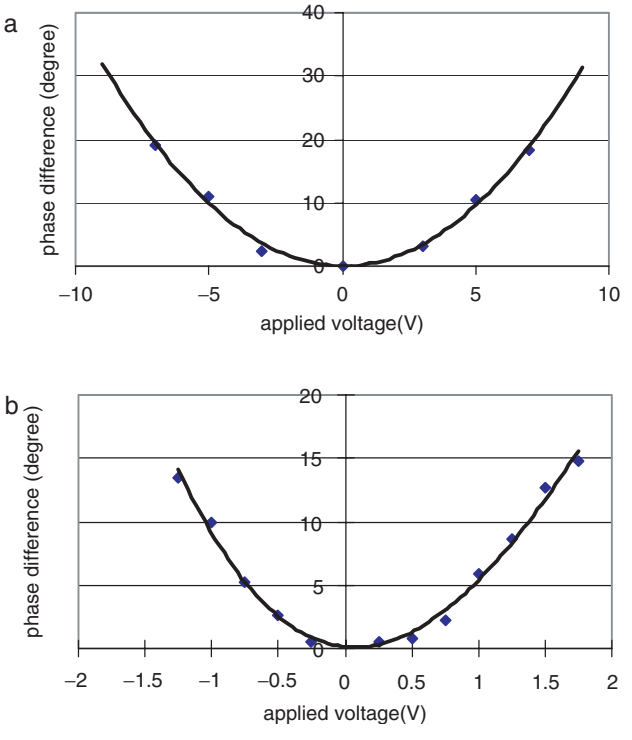

This figure is available in colour online.

Phase shifts plotted against the applied bias in the case of (**a**) a homogenous hydrophilic SAM (6-mercapto-1-hexanol) and (**b**) a homogeneous SAM composed of molecules with localized charges (1-(10-mercaptodecyl)-1′-methyl-4,4′-bipyridinium bis-chloride). The phase shift is defined as the absolute difference between the average phase values at a given applied bias minus the average phase value at zero bias. It should be noted that, in the case of neutral molecules, the curve is perfectly symmetrical and quadratic, while, in the case of molecules with localized charges, the plot is asymmetric. The continuous lines are fits to help the eye.

References

[1] A. Ulman. Self assembled monolayers, Chapter 2, in *Characterization of Organic Thin Films*, edited by C. A. Evans Jr (Butterworth-Heinemann, Boston, 1995).
[2] A. R. Bishop, and R. G. Nuzzo. Self-assembled monolayers: Recent developments and applications. Curr. Opin. Colloid Interface Sci. **1,** 127 (1996).
[3] M. Halik, H. Klauk, U. Zschieschang, G. Schmid, S. Ponomarenko, S. Kirchmeyer, and W. Weber. Relationship between molecular structure and electrical performance of oligothiophene organic thin film transistors. Adv. Mater. **15,** 917 (2003).
[4] M. Halik, H. Klauk, U. Zschieschang, G. Schmid, C. Dehm, M. Schutz, S. Maisch, F. Effenberger, M. Brunnbauer, and F. Stellacci. Low-voltage organic transistors with an amorphous molecular gate dielectric. Nature **431,** 963 (2004).
[5] N. C. Santos, and M. Castanho. An overview of the biophysical applications of atomic force microscopy. Biophys. Chem. **107,** 133 (2004).
[6] B. R. A. Neves, D. N. Leonard, M. E. Salmon, P. E. Russell, and E. B. Troughton. Observation of topography inversion in atomic force microscopy of self-assembled monolayers. Nanotechnol. **10,** 399 (1999).
[7] A. Noy, D. V. Vezenov, and C. M. Lieber. Chemical force microscopy. Ann. Rev. Mater. Sci. **27,** 381 (1997).
[8] M. Fujihira. Kelvin probe force microscopy of molecular surfaces. Ann. Rev. Mater. Sci. **29,** 353 (1999).
[9] J. B. D. Green, M. T. McDermott, M. D. Porter, and L. M. Siperko. Nanometer-scale mapping of chemically distinct domains at well-defined organic interfaces using frictional force microscopy. J. phys. Chem. **99,** 10960 (1995).
[10] M. F. Paige. A comparison of atomic force microscope friction and phase imaging for the characterization of an immiscible polystyrene/poly(methyl methacrylate) blend film. Polymer **44,** 6345 (2003).
[11] T. Takahashi and T. Kawamukai. Phase detection of electrostatic force by AFM with a conductive tip. Ultramicroscopy **82,** 63 (2000).
[12] H. Sugimura, K. Hayashi, N. Saito, O. Takai, and N. Nakagiri. Surface potential images of microstructured organosilane self-assembled monolayers acquired by Kelvin probe force microscopy. Jpn. J. Appl. Phys., Part 2 – Lett. **40,** L174 (2001).
[13] J. Lu, E. Delamarche, R. Bennewitz, E. Meyer, and H. J. Guntherodt. Kelvin probe force microscopy on surfaces: Investigation of the surface potential of self-assembled monolayers on gold. Langmuir **15,** 8184 (1999).
[14] A. S. Blum, C. M. Soto, C. D. Wilson, J. D. Cole, M. Kim, B. Gnade, A. Chatterji, W. F. Ochoa, T. W. Lin, J. E. Johnson, and B. R. Ratna. Cowpea mosaic virus as a scaffold for 3-D patterning of gold nanoparticles. Nano Lett. **4,** 867 (2004).
[15] H. Takano, S. S. Wong, J. A. Harnisch, and M. D. Porter. Mapping the subsurface composition of organic films by electric force microscopy. Langmuir **16,** 5231 (2000).
[16] J. W. Hong, S. I. Park, and Z. G. Khim. Measurement of hardness, surface potential, and charge distribution with dynamic contact mode electrostatic force microscope. Rev. Sci. Instrum. **70,** 1735 (1999).
[17] J. P. Cleveland, B. Anczykowski, A. E. Schmid, and V. B. Elings. Energy dissipation in tapping-mode atomic force microscopy. Appl. Phys. Lett. **72,** 2613 (1998).
[18] B. Basnar, G. Friedbacher, H. Brunner, T. Vallant, U. Mayer, and H. Hoffmann. Analytical evaluation of tapping mode atomic force microscopy for chemical imaging of surfaces. Appl. Surf. Sci. **171,** 213 (2001).
[19] P. J. James, M. Antognozzi, J. Tamayo, T. J. McMaster, J. M. Newton, and M. J. Miles. Interpretation of contrast in tapping mode AFM and shear force microscopy. A study of nafion. Langmuir **17,** 349 (2001).

[20] L. Nony, T. Cohen-Bouhacina, and J. P. Aime. Dissipation induced by attractive interaction in dynamic force microscopy: Contribution of adsorbed water layers. Surf. Sci. **499,** 152 (2002).
[21] I. Schmitz, M. Schreiner, G. Friedbacher, and M. Grasserbauer. Phase imaging as an extension to tapping mode AFM for the identification of material properties on humidity-sensitive surfaces. Appl. Surf. Sci. **115,** 190 (1997).
[22] P. Girard. Electrostatic force microscopy: Principles and some applications to semiconductors. Nanotechnol. **12,** 485 (2001).
[23] C. H. Lei, A. Das, M. Elliott, and J. E. Macdonald. Quantitative electrostatic force microscopy-phase measurements. Nanotechnol. **15,** 627 (2004).
[24] A. Sebastian, M. V. Salapaka, D. J. Chen, and J. P. Cleveland. Harmonic and power balance tools for tapping-mode atomic force microscope. J. Appl. Phys. **89,** 6473 (2001).
[25] J. Israelachvili. *Intermolecular and Surface Forces* (Academic Press, London, 1991).
[26] S. Hudlet, M. Saint Jean, C. Guthmann, and J. Berger. Evaluation of the capacitive force between an atomic force microscopy tip and a metallic surface. Eur. Phys. J. B **2,** 5 (1998).
[27] R. K. Smith, S. M. Reed, P. A. Lewis, J. D. Monnell, R. S. Clegg, K. F. Kelly, L. A. Bumm, J. E. Hutchison, and P. S. Weiss. Phase separation within a binary self-assembled monolayer on Au{111} driven by an amide-containing alkanethiol. J. phys. Chem. B **105,** 1119 (2001).
[28] A. M. Jackson, J. W. Myerson, and F. Stellacci. Spontaneous assembly of subnanometre ordered domains in the ligand shell of monolayer-protected nanoparticles. Nature Mater. **3,** 330 (2004).
[29] W. D. Schubert, O. Klukas, N. Krauss, W. Saenger, P. Fromme, and H. T. Witt. Photosystem I of Synechococcus elongatus at 4 angstrom resolution: Comprehensive structure analysis. J. Molec. Biol. **272,** 741 (1997).
[30] B. D. Bruce and R. Malkin. Subunit stoichiometry of the chloroplast photosystem-I complex. J. Bio. Chem. **263**, 7302 (1988).
[31] R. Das, P. J. Kiley, M. Segal, J. E. Norville, A. A. Yu, L. Wang, S. A. Trammell, L. E. Reddick, R. Kumar, F. Stellacci, N. Lebedev, J. Schnur, B. D. Bruce, S. Zhang, and M. Baldo. Integration of photosynthetic protein molecular complexes in solid-state electronic devices. Nano Lett. **4,** 1079 (2004).
[32] This work was done using higher plant PSI preparations. These complexes are not believed to be a trimer in their native membrane [Ref 29. P. Jordan, *et al.*, Three-dimensional structure of cyanobacterial photosystem I at 2.5 A resolution. Nature **411**(6840), 909–17 (2001)]. However, upon isolation and immobilization in a non-aqueous, solid state, they may tend to form trimers that are the result of hydrophobic interactions. Whether the observed trimers are structurally equivalent to the cyanobacterial "native" trimer [P. Jordan *et al.*, Three-dimensional structure of cyanobacterial photosystem I at 2.5 A resolution. Nature **411**(6840), 909–17 (2001).] is not known, however the presence of four or more LHC1 subunits associated with the plant PSI prep [A. Ben-Shem, F. Frolow, and N. Nelson. Crystal structure of plant photosystem I. Nature **426**(6967), 630–5 (2003)], may require that those subunits be positioned on the "outside" edge, facing the trimeric perimeter. The three islands observed in the difference image may actually represent the highly charged region of psaF lumenal surface that function as an electrostatic docking site for the primary electron donor, plastocyanin [R. M. Wynn and R. Malkin. Interaction of plastocyanin with photosystem I: a chemical cross-linking study of the polypeptide that binds plastocyanin. Biochemistry **27**(16), 5863–9 (1988). M. Hippler, *et al.*, The plastocyanin binding domain of photosystem I. Embo. J. **15**(23), 6374–84 (1996)]. However the "native" trimeric orientation is unlikely when the data is compared to cyanobacterial trimeric PSI complexes, which would separate the charged regions of each psaF by at least 15nm. Alternatively, an inverted trimer (LHC core as opposed to LHC periphery) distances the implicated region of psaF by ~10nm (Data not shown). The observation that the EPTA signal is positively influence by hydration could be explained by the presence of tightly bound water layer over this charged region of the lumenal surface of PSI. Similar experiments performed following the docking of the plastocyanin subunit to this region could help explain the molecular basis of this observation [S. V. Ruffle, *et al.*, The location of plastocyanin in vascular plant photosystem I. J. Biol. Chem. 277(28), 25692–6 (2002)]. In addition, analysis of PSI complexes that are immobilized in the opposite orientation, i.e. stromal "hump" facing up could also provide further insight into the origin of this EPTA signal.